Nuclear Instruments and Methods in Physics Research A245 (1986) 27–34
North-Holland, Amsterdam

HADRON SHOWER PUNCHTHROUGH FOR INCIDENT HADRONS OF MOMENTUM 15, 25, 50, 100, 200 AND 300 GeV/*c*

F.S. MERRITT, M. OREGLIA, H. SCHELLMAN and B.A. SCHUMM

Enrico Fermi Institute, University of Chicago, Chicago, IL 60637, USA

K.T. BACHMANN, R.H. BERNSTEIN, R.E. BLAIR, C. FOUDAS, W.C. LEFMANN, S.R. MISHRA, E. OLTMAN, F. SCIULLI, M.H. SHAEVITZ and W.H. SMITH

Physics Department, Columbia University, New York, NY 10027, USA

F. BORCHERDING, H.E. FISK, D. YOVANOVITCH, M.J. LAMM, W. MARSH, K.W.B. MERRITT and P.A. RAPIDIS

Fermi National Accelerator Laboratory, Batavia, IL 60510, USA

A. BODEK, H.S. BUDD and W.K. SAKUMOTO

Department of Physics and Astronomy, University of Rochester, Rochester, NY 14627, USA

Received 1 November 1985

We present data on the punchthrough probability for showers of positively charged hadrons with momenta 15, 25, 50, 100, 200, and 300 GeV/*c*. Data were taken using the CCFR neutrino detector (the Lab E detector), an iron calorimeter instrumented with counters every 10 cm of iron, and drift chambers every 20 cm of iron.

1. Introduction

Data on hadronic punchthrough and shower lengths are important for many experiments. For example, the identification of muons in colliding beam detectors relies on muon penetration through a hadron absorber. The identification of neutrino induced neutral current events relies on the absence of a penetrating particle through a hadron absorber. In muon and neutrino interactions, understanding the sources of background for prompt single muon, dimuon, and multimuon events is crucial. Therefore, the probability of hadronic punchthrough across absorbers of various lengths must be understood.

The punchthrough data we present were obtained as a byproduct of an energy calibration run for our calorimeter using a hadron beam. We report only on a small subset of our data, which are the low beam intensity (less than 5000 particles per 6 s spill) unbiased interactions. In this report, we present integrated hadronic punchthrough probabilities as a function of penetration depth from the start of our calorimeter. Punchthrough probabilities as a function of the length from the start of the multiparticle hadronic cascade will be presented in a later communication.

0168-9002/86/$03.50

2. Experimental setup

The NTW (neutrino test west) beam line at Fermilab was used to deliver the hadrons. Primary 800 GeV/*c* protons from the Tevatron were targeted on a one-interaction-length aluminum target. Secondary charged particles produced at angles between 0 and 10 mrad were transported to the detector by the NTW beam line. The secondary beam could be charge and momentum selected between 10 and 450 GeV/*c*. For almost all of the calibration run, positively charged particles were selected.

Hadrons in the momentum selected secondary beam were also momentum analyzed using the spectrometer located at the far upstream end of the detector. This spectrometer consisted of four multiwire proportional chambers, two closely spaced analyzing magnets, and one drift chamber (see fig. 1). The momentum spread (σ_p) of the beam varied from 7% at 15 GeV/*c* to about 2% at 100 GeV/*c* and higher. A small scintillation counter (called UV2) located at an aperture of the magnet provided timing information. The calorimeter consisted of 3 m $\times$ 3 m $\times$ 5.2 cm steel plates interspersed with liquid scintillation counters placed every 10 cm of steel and drift chambers every 20 cm of steel

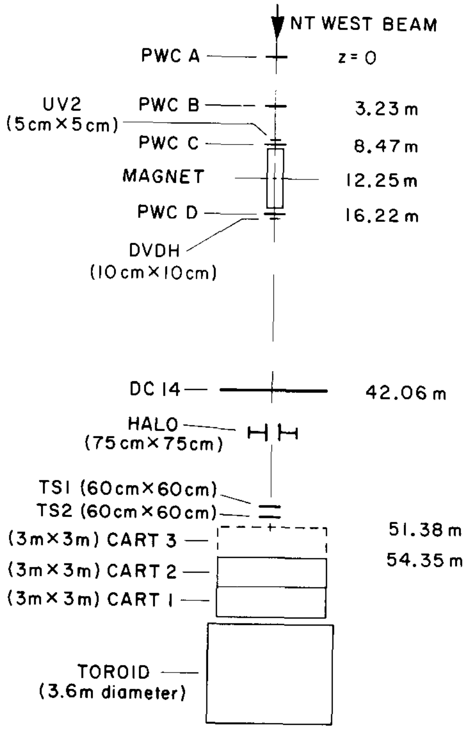

Fig. 1. Plan view of the experimental setup. The spectrometer system, which is used to measure the momentum of incoming hadrons, contains two bending magnets, four MWPCs, and a drift chamber. Counter UV2 is used for timing.

(see fig. 2). A submodule of the calorimeter consists of the following elements: a 5.2 cm thick steel plate, an average of about 6.2 cm of space for a liquid scintillation counter, two 5.2 cm steel plates, another 6.2 cm of space for a liquid scintillation counter, a 5.2 cm steel plate, and finally, 9 cm of space for a drift chamber station. Therefore, the total material in a submodule includes 20.6 cm of steel over a distance of about 42 cm. Seven of these submodules are mounted on a movable tray called a "target cart".

Each cart has fourteen counters and slots for six drift chamber stations. The full calorimeter consists of six carts. During this test run, only the two most downstream carts (Carts 1 and 2), were instrumented with drift chambers. The next upstream cart (Cart 3) was partially filled with uninstrumented drift chambers. Its three upstream drift chamber stations were empty. Drift chamber stations were also located in the space between Carts 1 and 2 and between Carts 2 and 3 so that the periodicity of material was maintained from cart to cart. The only difference was that the space for the drift chamber station between the carts was about 2 cm larger than that for the spaces within the cart. All target carts were independently movable. The target configuration for the data being presented was: Carts 1 and 2, always in the beam; Cart 3, in the beam for much of the data taking; Carts 4 to 6, out of the beam. Including all material, the configuration with all three downstream carts in the beam has an average target density of 4.19 g/cm^3, and the corresponding average interaction length is 1.80 λ_{Fe}, where λ_{Fe} is the interacation length of solid iron.

The liquid scintillation counters have an active area of 3×3 m^2. There are wavelength shifter bars along each edge and phototubes on each corner. For a muon traversing the center of the counter, the pulse amplitude of the sum of the four corner phototubes corresponds to about 10 photoelectrons. The timing information for the discriminated phototube output of each counter was measured using the same time to digital converters (TDCs) that were used for the drift chambers. Analog outputs were measured by LRS 4300 FERA analog to digital converters (ADCs).

The drift chambers had an active area of 3×3 m^2 with 24 horizontal and 24 vertical cells. Each cell was 12.7 cm wide by 1.9 cm high by 3 m long. There were three wire cells with a central 0.13 mm diameter field wire and two 0.03 mm diameter sense sires spaced 2 mm on each side. The three-wire geometry resolves left–right ambiguities. The hit information was buffered into multihit TDCs and read out for each event.

3. Analysis

The event trigger used in this analysis was the coincidence between the incident beam signal from the small timing counter UV2, and an energy deposition signal from the calorimeter. Only data taken with low incident beam intensities and with the beam targeted onto the center of our calorimeter were used. This yields a cleaner sample of unbiased hadronic interactions. In addition, we selected events having just a single hadron showering within the calorimeter. Single particle events were selected by using the UV2 timing counter and the proportional wire chambers of the magnetic spectrometer upstream of our detector. Beam related halo particles and any upstream showers were suppressed by using the upstream drift chamber as a veto counter (see fig. 1). Events with more than one hit in both the x and y views of this drift chamber were rejected. In addition, only one hit was allowed in the beam region, and it had to be consistent with the beam particle. Because this will not eliminate halo muons accompanying the hadron with a 100% efficiency, we manually scanned long shower length event displays to identify non-shower-related tracks.

There was some fraction of electrons and muons in our beam. At 15 and 25 GeV/c, there was a sizable electron contamination of the beam. The electrons were identified by looking at the ratio of the shower energy

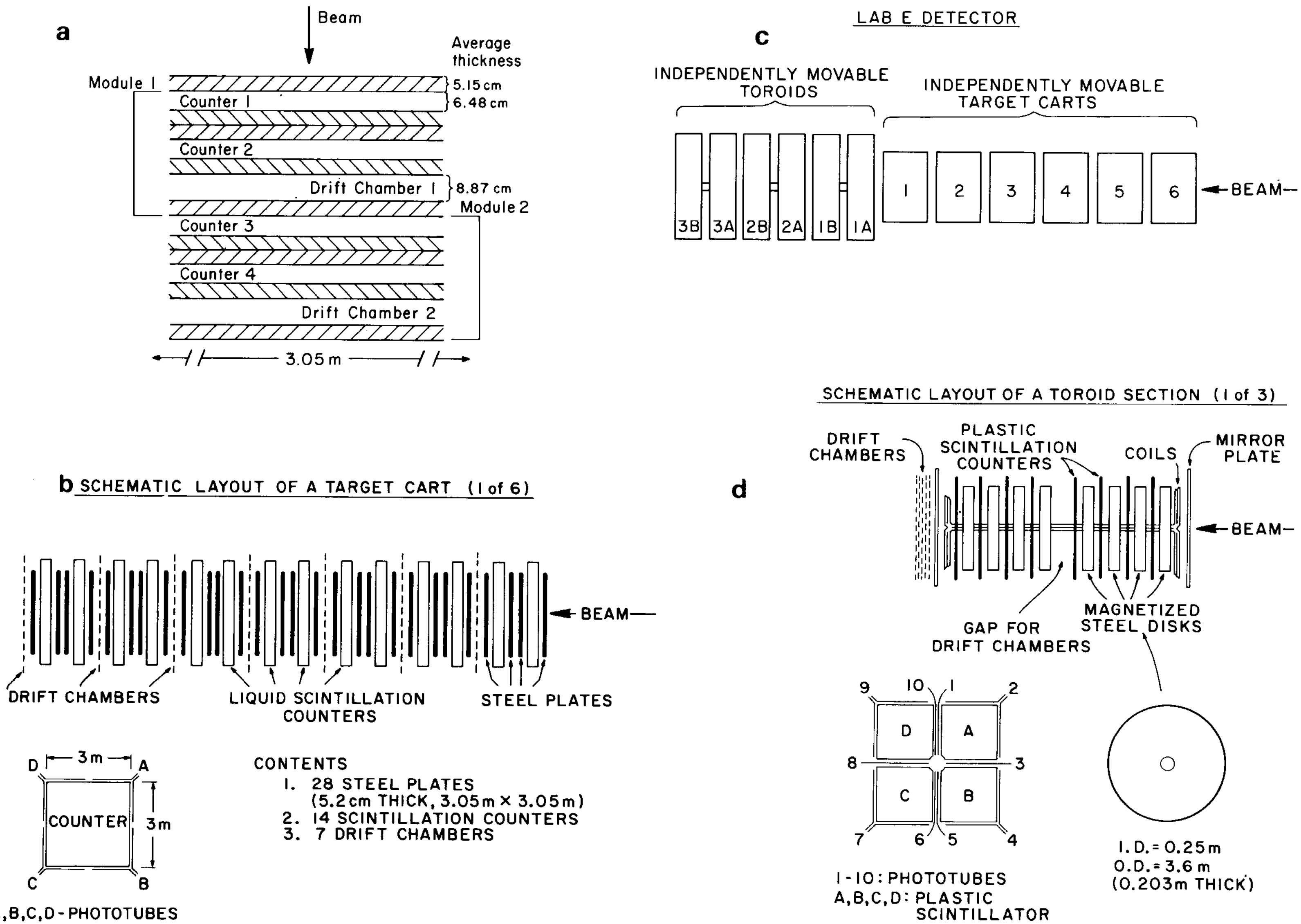

Fig. 2. Details of the calorimeter. (a) Two submodules containing steel plates, counters and drift chambers. A cart consists of seven submodules. (b) A complete calorimeter cart (not to scale) containing 28 5 cm thick plates of iron, 14 scintillation counters and 7 drift chambers. (c) The experimental layout (not to scale) showing the six movable target carts followed by a muon spectrometer. For these data, Carts 4, 5, 6 were out of the beam. (d) The layout (not to scale) of one of the three toroids of the muon spectrometer.

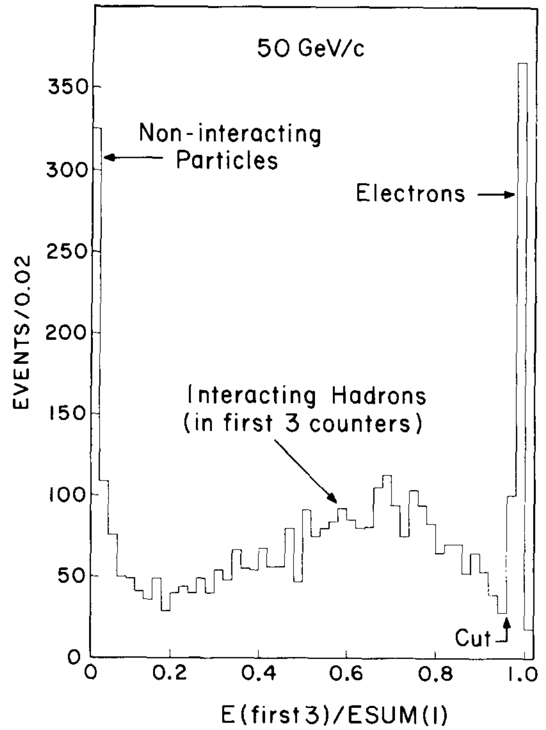

Fig. 3. The distribution of the ratio between the energy in the three most upstream counters and total energy contained within the shower boundaries. Electrons have a ratio close to 1, noninteracting particles populate the region near 0 and hadron interactions populate the region between 0 and 1.

measured in the first three exposed counters to the total energy. For electrons this ratio is close to 1, for interacting hadrons, it is distributed between 0 and 1, and for noninteracting hadrons, the ratio is close to 0 (see fig. 3). This is true because electromagnetic showers are much shorter than hadronic showers.

Muons that pass the trigger requirements will most likely span the full length of the target carts within the beam line and deposit some electromagnetic shower energy somewhere within that region. This topology was used to identify the beam muons. A cut made on the total energy deposited in the calorimeter also helped to eliminate beam muons.

For beam momenta under 25 GeV/c, the electron contamination was well over 50% and not acceptable. During much of the 15 GeV/c running we enhanced the fraction of hadrons incident on the calorimeter by placing a 10 cm lead "filter" within the beam at a position ahead of the upstream magnetic spectrometer. Data from the "filtered" 15 GeV/c running are presented in this communication.

4. Results

We define the shower length to be the penetration depth into the calorimeter of the final particles in the hadron induced shower. The penetration depth is given in terms of the most downstream scintillation counter with any activity, i.e., discriminator hits corresponding to a threshold setting of about 25% minimum ionizing. This does not ensure that a charged particle going into the counter produced the activity. Neutrons can activate the counters as well. All depths given are with respect to the start of our calorimeter.

Because our calorimeter is not homogeneous, we also give the depth of the counter in terms of an equivalent length of a uniform block of steel. Note that the number of interaction lengths, the total dE/dx energy loss,

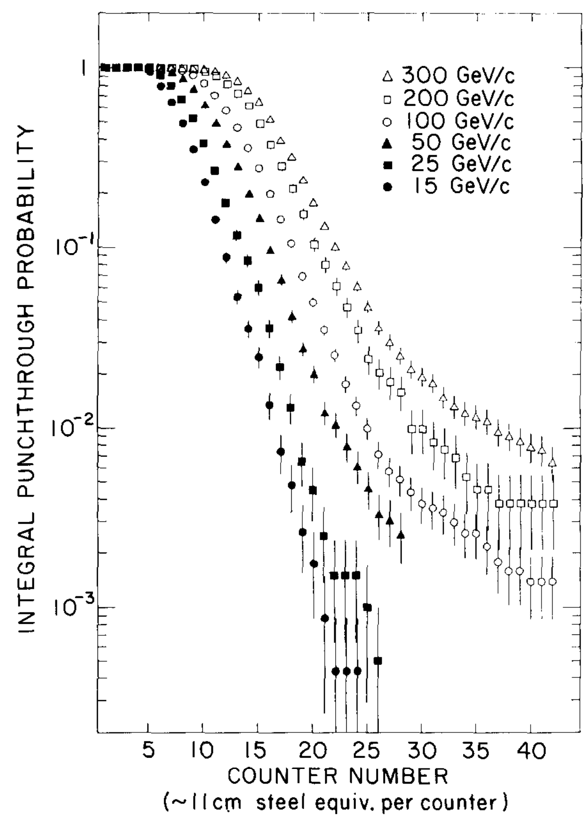

Fig. 4. The integral probability distributions for hadronic shower punchthrough as a function of depth in terms of counter number. The curves for 15, 25 and 50 GeV/c are for the "2 cart" configuration, and for 100, 200 and 300 GeV/c are for the "3 cart" configuration. The corresponding depth in terms of steel equivalent in front of each counter is given in table 1. There is approximately 11 cm of steel equivalent between counters. The punchthrough probability for a given counter is the fraction of hadron showers for which the shower penetration is equal to or greater than the depth of that counter.

and the average density of the absorber are the relevant parameters [1] when data for absorbers of different materials and different configurations are compared. Most of the material in the calorimeter is iron, and the small amount of material from the counters and drift chambers has been converted to iron equivalent distances.

These iron equivalent amounts in front of each counter number are given in tables 1a and 1b. The first column is the counter number from the start of the detector and the values given for each counter are the total amount of material from the beginning of the calorimeter to the front face of that counter. The basic periodicity of the calorimeter repeats every two counters. The material between an even numbered counter and an odd numbered counter consists of two plates of steel, while the material between an odd numbered counter and an even numbered counter consists of two steel plates and a drift chamber. Table 1a is for the calorimeter configuration with Cart 2 as the first target cart exposed to the beam ("2 cart": $\lambda = 1.80\lambda_{Fe}$, $\rho = 4.20$ g/cm^3). Table 1b is the configuration with Cart 3 being the first exposed target cart ("3 cart": $\lambda = 1.81\lambda_{Fe}$, $\rho = 4.18$ g/cm^3). They vary slightly because the three

Table 1a
Steel equivalent for the "2 cart" configuration, $\rho = 4.20$ g/cm^3, $\lambda = 1.80\lambda_{Fe}$ (first 9 interaction lengths)

Counter	Nominal distance from entry [cm]	Interaction lengths		Muon range	
		Steel equiv. [cm]	[λ's]	Steel equiv. [cm]	Momentum [GeV/c]
1	5.2	5.2	0.3	5.2	0.2
2	22.9	16.7	1.0	16.5	0.3
3	45.8	28.7	1.7	28.2	0.5
4	63.6	40.3	2.4	39.6	0.6
5	89.0	52.2	3.1	51.3	0.7
6	104.2	63.8	3.8	62.7	0.9
7	129.6	75.7	4.5	74.4	1.0
8	147.4	87.3	5.2	85.8	1.2
9	172.8	99.3	5.9	97.5	1.3
10	190.6	110.8	6.6	108.9	1.5
11	213.4	122.8	7.3	120.6	1.6
12	231.2	134.4	8.0	131.9	1.8
13	256.6	146.3	8.7	143.6	1.9
14	274.4	157.9	9.4	155.0	2.1
15	302.3	169.8	10.1	166.7	2.2
16	317.6	181.4	10.8	178.1	2.4
17	343.0	193.4	11.5	189.8	2.5
18	360.8	204.9	12.2	201.2	2.7
19	386.2	216.9	12.9	212.9	2.9
20	401.4	228.5	13.6	224.3	3.0
21	426.8	240.4	14.3	236.0	3.2
22	444.6	252.0	15.0	247.3	3.3
23	467.4	263.9	15.7	259.0	3.5
24	485.2	275.5	16.4	270.4	3.7
25	510.6	287.5	17.2	282.1	3.8
26	528.4	299.0	17.8	293.5	4.0
27	553.8	311.0	18.6	305.2	4.2
28	569.0	322.6	19.2	316.6	4.3

Table 1b
Steel equivalent for the "3 cart" configuration, $\rho = 4.18$ g/cm^3, $\lambda = 1.81\ \lambda_{Fe}$ (first 9 interaction lengths)

Counter	Nominal distance from entry [cm]	Interaction lengths		Muon range	
		Steel equiv. [cm]	[λ's]	Steel equiv. [cm]	Momentum [GeV/c]
1	5.2	5.2	0.3	5.2	0.2
2	22.9	16.7	1.0	16.5	0.3
3	48.3	28.3	1.7	27.9	0.5
4	63.6	39.9	2.4	39.3	0.6
5	89.0	51.5	3.1	50.7	0.7
6	106.8	63.1	3.8	62.1	0.9
7	132.2	74.6	4.5	73.5	1.0
8	147.4	86.2	5.1	84.8	1.2
9	172.8	98.2	5.9	96.5	1.3
10	190.6	109.7	6.5	107.9	1.5
11	216.0	121.7	7.3	119.6	1.6
12	231.2	133.3	8.0	131.0	1.8
13	256.6	145.2	8.7	142.7	1.9
14	274.4	156.8	9.4	154.1	2.1
15	302.3	168.7	10.1	165.8	2.2
16	320.1	180.3	10.8	177.2	2.4
17	343.0	192.3	11.5	188.9	2.5
18	360.8	203.8	12.2	200.2	2.7
19	386.2	215.8	12.9	211.9	2.9
20	401.4	227.4	13.6	223.3	3.0
21	426.8	239.3	14.3	235.0	3.2
22	444.6	250.9	15.0	246.4	3.3
23	470.0	262.8	15.7	258.1	3.5
24	487.8	274.4	16.4	269.5	3.7
25	510.6	286.4	17.1	281.2	3.8
26	528.4	298.0	17.8	292.6	4.0
27	553.8	309.9	18.5	304.3	4.2
28	571.6	321.5	19.2	315.6	4.3
29	599.5	333.4	19.9	327.3	4.5
30	614.8	345.0	20.6	338.7	4.7
31	640.2	356.9	21.3	350.4	4.8
32	657.9	368.5	22.0	361.8	5.0
33	683.3	380.5	22.7	373.5	5.2
34	698.6	392.1	23.4	384.9	5.3
35	724.0	404.0	24.1	396.6	5.5
36	741.8	415.6	24.8	408.0	5.7
37	764.6	427.5	25.5	419.7	5.8
38	782.4	439.1	26.2	431.0	6.0
39	807.8	451.1	26.9	442.7	6.2
40	825.6	462.6	27.6	454.1	6.3
41	851.0	474.6	28.3	465.8	6.5
42	866.2	486.2	29.0	477.2	6.7

most upstream drift chamber positions in Cart 3 were empty. The second column gives the absolute distance from the start of the calorimeter. The third column gives the interaction length as the equivalent depth in a uniform steel block. The fourth column gives the number of proton interaction lengths. The fifth column is the range of a muon, expressed as an equivalent distance in steel. The last column gives this range [2] in GeV/c.

Tables 2a and 2b give the integral distribution of the penetration depths. Each row gives the number of showers whose penetration depth was equal to or larger than the depth shown in terms of counter number. Table 2a gives the integral distribution for 15, 25, and 50 GeV/c. This is only with the "2 cart" configuration. Table 2b gives those integral distributions for 100, 200, and 300 GeV/c, for both the "2 cart" and "3 cart" configurations. Tables 3a and 3b give the respective hadronic punchthrough probabilities. The statistical errors on these quantities can be extracted from the number of events in tables 2a and 2b. Fig. 4 shows a plot of these punchthrough probabilities.

For most of the data in these tables, only counter information was used. However, for each beam energy, we manually scanned the event display of all showers with fairly large penetration depths. Since these event displays contained drift chamber and counter information, events with particle tracks that were not associated with the tagged beam hadron's shower could be easily identified. We scanned 273 deep penetration events. One contained a non-shower-related beam halo muon, one contained a cosmic ray muon, and the rest were perfectly acceptable. The negligible level of accidental

Table 2a
Integral distribution, hadron shower penetration for 15, 25, and 50 GeV/c ("2 cart" configuration)

Counter	15 GeV/c	25 GeV/c	50 GeV/c
1	2299	2002	3929
2	2299	2002	3929
3	2299	2002	3929
4	2299	2002	3929
5	2182	1973	3925
6	1826	1828	3855
7	1488	1602	3721
8	1128	1348	3452
9	807	1044	3015
10	528	758	2454
11	329	539	1949
12	202	354	1492
13	123	234	1113
14	82	168	781
15	57	120	572
16	31	72	380
17	17	44	261
18	11	26	165
19	6	13	109
20	4	9	79
21	2	5	48
22	1	3	41
23	1	3	31
24	1	3	24
25	0	2	18
26	0	1	13
27	0	0	12
28	0	0	10

Table 2b
Integral distribution, hadron shower penetration for 100, 200, and 300 GeV/c

Counter	100 GeV/c		200 GeV/c		300 GeV/c
	2 cart	3 cart	2 cart	3 cart	3 cart
1	1506	5044	5272	1321	3556
2	1506	5044	5272	1321	3556
3	1506	5044	5272	1321	3556
4	1506	5044	5272	1321	3556
5	1506	5044	5272	1321	3556
6	1498	5025	5267	1320	3556
7	1489	4983	5257	1316	3553
8	1456	4862	5230	1311	3549
9	1397	4608	5172	1300	3536
10	1291	4141	5060	1255	3499
11	1143	3575	4864	1199	3427
12	962	2934	4526	1079	3275
13	731	2353	3981	953	3028
14	580	1806	3366	814	2693
15	455	1389	2826	646	2320
16	325	1002	2199	495	1853
17	221	723	1689	375	1413
18	152	531	1286	280	1141
19	107	349	963	201	847
20	67	251	730	137	630
21	44	178	495	106	470
22	32	129	374	81	361
23	22	89	263	62	281
24	16	67	190	46	217
25	11	50	150	32	168
26	7	36	123	27	129
27	6	29	108	24	107
28	3	26	89	21	90
29	–	22	–	13	76
30	–	19	–	13	69
31	–	18	–	11	64
32	–	17	–	10	53
33	–	15	–	9	47
34	–	13	–	7	43
35	–	13	–	6	41
36	–	11	–	6	39
37	–	9	–	5	34
38	–	8	–	5	32
39	–	8	–	5	30
40	–	7	–	5	28
41	–	7	–	5	27
42	–	7	–	5	23

background was due to the low beam intensity for these data. In a large fraction of these deep penetration events, a muon emerging from the body of the hadronic shower was the final particle at the downstream end of the shower.

5. Discussion

A hadron shower cascade contains a small fraction of muons. These muons are primarily from the weak decays in flight of unstable hadrons. The absorption of hadron shower cascades were shown in the integral punchthrough probability distributions of fig. 4. Because muons penetrate through matter much more effectively than hadrons, the integral punchthrough probability distributions of fig. 4 have two distinct regions of exponential falloff, especially for beam energies above 100 GeV/c. In the region immediately after the flat top, the majority of punchthrough particles are hadrons. Hence, the exponential falloff in this region reflects the absorption of hadrons. The integral hadron punchthrough probability in this region depends primarily on the number of absorption lengths from the start on the calorimeter.

In the next region, the majority of punchthrough particles are decay muons. The integral punchthrough probability curves indicate that the number of deeply penetrating muons depends on the incident hadron energy. The muon range depends on energy and on the material and structure of the calorimeter. As these muons are primarily from the weak decays in flight of π's and

Table 3a
Integral probability distribution, hadron shower penetration for 15, 25, and 50 GeV/c ("2 cart" configuration)

Counter	15 GeV/c [%]	25 GeV/c [%]	50 GeV/c [%]
1	100.0	100.0	100.0
2	100.0	100.0	100.0
3	100.0	100.0	100.0
4	100.0	100.0	100.0
5	94.9	98.6	99.9
6	79.4	91.3	98.1
7	64.7	80.0	94.7
8	49.1	67.3	87.9
9	35.1	52.1	76.7
10	23.0	37.9	62.5
11	14.3	26.9	49.6
12	8.8	17.7	38.0
13	5.4	11.7	28.3
14	3.6	8.4	19.9
15	2.5	6.0	14.6
16	1.3	3.6	9.7
17	0.7	2.2	6.6
18	0.5	1.3	4.2
19	0.3	0.7	2.8
20	0.2	0.5	2.0
21	0.1	0.3	1.2
22	0.04	0.2	1.0
23	0.04	0.2	0.8
24	0.04	0.2	0.6
25	0.0	0.1	0.5
26	0.0	0.05	0.3
27	0.0	0.0	0.3
28	0.0	0.0	0.3

Table 3b
Integral probability distribution, hadron shower penetration for 100, 200, and 300 GeV/c

Counter	100 GeV/c [%]		200 GeV/c [%]		300 GeV/c [%]
	2 cart	3 cart	2 cart	3 cart	3 cart
1	100.0	100.0	100.0	100.0	100.0
2	100.0	100.0	100.0	100.0	100.0
3	100.0	100.0	100.0	100.0	100.0
4	100.0	100.0	100.0	100.0	100.0
5	100.0	100.0	100.0	100.0	100.0
6	99.5	99.6	99.9	99.9	100.0
7	98.9	98.8	99.7	99.6	99.9
8	96.7	96.4	99.2	99.2	99.8
9	92.8	91.4	98.1	98.4	99.4
10	85.7	82.1	96.0	95.0	98.4
11	75.9	70.9	92.3	90.8	96.4
12	63.9	58.2	85.9	81.7	92.1
13	48.5	46.6	75.5	72.1	85.2
14	38.5	35.8	63.9	61.6	75.7
15	30.2	27.5	53.6	48.9	65.2
16	21.6	19.9	41.7	37.5	52.1
17	14.7	14.3	32.0	28.4	39.7
18	10.1	10.5	24.4	21.2	32.1
19	7.1	6.9	18.3	15.2	23.8
20	4.5	5.0	13.9	10.4	17.7
21	3.0	3.5	9.4	8.0	13.2
22	2.1	2.6	7.1	6.1	10.2
23	1.5	1.8	5.0	4.7	7.9
24	1.1	1.3	3.6	3.5	6.1
25	0.7	1.0	2.9	2.4	4.7
26	0.5	0.7	2.3	2.0	3.6
27	0.4	0.6	2.1	1.8	3.0
28	0.2	0.5	1.7	1.6	2.5
29	–	0.4	–	1.0	2.1
30	–	0.4	–	1.0	1.9
31	–	0.4	–	0.8	1.8
32	–	0.3	–	0.8	1.5
33	–	0.3	–	0.7	1.3
34	–	0.3	–	0.5	1.2
35	–	0.3	–	0.5	1.2
36	–	0.2	–	0.5	1.1
37	–	0.2	–	0.4	1.0
38	–	0.2	–	0.4	0.9
39	–	0.2	–	0.4	0.8
40	–	0.1	–	0.4	0.8
41	–	0.1	–	0.4	0.8
42	–	0.1	–	0.4	0.6

K's, the punchthrough probability in this region depends not only on the range properties of the material in front of this region, but also on the structure of the calorimeter. The regions of the calorimeter which are instrumented with counters or drift chambers have lower density. Within these regions, shower hadrons have a larger decay probability into muons.

When comparing muon punchthrough data from one calorimeter to another, the following empirical formula for the integrated muon punchthrough probability can be used [1].

$$P = (p/350\ \text{GeV})\left[0.0095\ \mathrm{e}^{-1.43(\sqrt{R}-2)}\right] \times (0.22 + 0.59\lambda/\lambda_{\mathrm{Fe}}).$$

The expression is a crude fit to data from other experiments for incident hadron momenta (p) between 75 and 400 GeV/c, and for identified muons with a $\mathrm{d}E/\mathrm{d}x$ total energy loss range (R) between 4 and 9 GeV/c. This formula agrees roughly with our data for penetration depths larger than 32 counters (or equivalently, for $R > 5.2$ GeV/c). In this region, most of our punchthrough particles are decay muons.

Appendix

A description of the various analysis cuts

(1) *Timing cuts.* The beam pulse timing (from UV2) had to be within ± 0.5 rf buckets (18 ns per rf bucket) of that tagged by the calorimeter trigger. There also had to be no other beam particles within 1 μs of it. (The width of the UV2 timing pulse was 100 ns). To ensure that the shower data for each scintillation counter were related to the tagged beam particle, the timing of each counter had to be within ± 2 rf buckets of the tagged beam pulse.

(2) *Clean beam cuts.* Only a single beam particle trajectory was allowed within the upstream magnetic spectrometer. There had to be only one track within the proportional wire chambers upstream of the magnet. Upstream showers were rejected by requiring only one hit within the upstream drift chamber (in either the x or y view), and that its location be consistent with the beam position.

(3) *Shower boundaries.* We looked for shower structure above two pulse height threshold levels. For structure at the single minimum ionizing level or larger, discriminator hits (threshold of 25% of minimum ionizing) were used to find the shower boundaries. The shower energy within this boundary is called ESUM(1). An event with two shower clusters separated by more than two nonactive counters was rejected. We defined the multiparticle cascade regions to be that portion where the counter pulse heights were above three times minimum ionizing. The total shower energy within these regions is called ESUM(M).

(4) *Muon cuts.* Any event where a particle penetrates to within 3 counters of the end of the calorimeter, and where there is a single multiparticle region of width less than or equal to 4 counters is rejected as a probable beam muon. Also, the shower energy (ESUM(1) for momenta larger than 50 GeV/c, ESUM(M) for momenta below that) was required to be consistent with the beam energy.

(5) *Electron cut.* Define R3 = (shower energy in first 3 counters)/ESUM(1). Events with R3 $\geqq 0.96$ are rejected as electrons (see fig. 3). For the 15 GeV/c data, a small fraction of the hadrons are misidentified as electrons. This misidentification error is at least a factor of 2 smaller than the statistical error.

References

[1] For scaling laws for absorbers of different materials, and for a summary of other data on hadronic punchthrough, see A. Bodek, University of Rochester preprint UR911 (1985); to be published in Proc. Workshop for Muon Identification at the SSC, Madison, Wisconsin (1985).

[2] G. Koizumi, Fermilab TM-786 (9 May 1978).